Rakenteiden Mekaniikka (Journal of Structural Mechanics)

Vol. 58, No. 4, 2025, pp. 186–196

https://rakenteidenmekaniikka.journal.fi/index

https://doi.org/10.23998/rm.149406

© 2025 The Authors

Open access under the license CC BY 4.0



Analysis of flow behavior of bioinks outside the 3D-printing nozzles

Ashish Pawar¹, Ashvinkumar Chaudhari and Eero Immonen

Summary The major challenge in extrusion-based bioprinting for medical application is printability, which largely depends on the flow behavior of bioinks just outside the nozzle. This flow behavior is influenced by several factors, including nozzle dimensions, bioink density, bioink viscosity, surface tension of the bioink-air interface, and the desired printing speed and structure. Accurately predicting the flow behavior of bioinks outside the nozzle in advance can reduce the costs associated with experimental testing. In this work, Volume of Fluid (VOF) method under Finite Volume method (FVM) framework is used to study the flow behavior outside a single nozzle. Computational Fluid Dynamics (CFD) simulations are conducted to analyze the behavior of bioinks outside the printing nozzles and flow behaviors are compared with literature. Initial simulations are performed using water due to its well characterized rheological and physical properties, and its widespread use as a reference medium in bioink formulations. The effect of all process parameters on the flow outside the nozzle was analyzed using water as the working fluid. By applying two non-dimensional numbers, Reynolds number and Weber number, flow demarcation regimes are established for water. Furthermore, simulations are performed for boinks to predict their printability. The model predictions for the qualitative flow behavior of bioinks at different temperatures matches well with experimental data from the literature.

Keywords: bioinks, 3D-printing, CFD, non-Newtonian, VOF

Received: 1 November 2024. Accepted: 15 July 2025. Published online: 27 October 2025

Introduction

3D printing (3DP) has revolutionized industrial mechanical design by creation of highly customizable, lightweight products and facilitating rapid prototyping. Recently, 3D bioprinting has gained more attention as well. 3DP enables the use of multicomponent materials and complex geometries, which are difficult to manufacture using conventional methods. These advancements hold promise for producing both improved 'one-size-fitsall' products (e.g., better efficacy, fewer side effects) and personalized medication.

To fully leverage the potential and flexibility of 3DP in the pharmaceutical industry, it is essential to understand the entire transport path of substances, from raw materials through 3DP processes to the patient. This necessitates the development of numerical models (e.g., rheology and fluid flow) to capture the underlying mechanisms. Classical Newtonian laws cannot predict bioinks (non-Newtonian material) properties. Hence, a

¹Corresponding author: ashish.pawar@turkuamk.fi

non-Newtonian model is necessary for accurately predicting complex fluid properties, such as shear-thickening/thinning, viscoelastic behavior, yield stress, etc. [1].

Attempts have been made to understand the flow behavior of non-Newtonian materials inside the nozzle by utilizing a Computational Fluid Dynamics (CFD) approach [2, 3]. These studies describe the relationship between fluid material properties and geometric parameters, as well as the suitability of different viscosity models. However, to assess the printability of particular bioinks, it is essential to predict flow behavior just outside the nozzle [4]. Furthermore, material and setup costs can be reduced if one can predict bioink flow behavior outside the nozzle without conducting physical experiments.

Cendrowski et al. [5] and Liravi et al. [6] used the Finite Volume Method (FVM) and Finite Element Method (FEM), respectively, to predict flow behavior outside the nozzle. Cendrowski et al. [5] conducted their analysis on Newtonian materials using the Volume of Fluid (VOF) method, while Liravi et al. [6] used the Carreau-Yasuda viscosity model for viscosity characterization and employed the level-set method to capture the interface between two fluids. The level set method uses signed distance function to define the interface. Finite Volume Method (FVM) is a numerical method for solving partial differential equations, in present case Navier-Stokes equations which are governing the physics of fluid motion. VOF is a interface tracking method specifically designed for tracking and locating the interface between two immiscible fluids [7]. It uses a volume fraction to track the position and evolution of the interface between the fluids. VOF can be used within FVM framework, where FVM solves the governing equations, and VOF tracks the fluid interfaces. There are many experimental studies available which discuss flow behavior of biomaterial outside the printing nozzle [4, 8, 9, 10].

To the best of the author's knowledge, apart from aforementioned studies no other computational studies are available in the literature that describe the flow behavior of non-Newtonian materials outside a nozzle and predict the printability of these materials. To address this gap, the present research utilizes a multiphase computational model solved by VOF method under FVM framework to analyze the flow behavior of bioinks (non-Newtonian) outside the nozzle. The computational results are compared with experimental data available in the literature. Using the proposed computational model, flow regimes are defined for water, and the flow behavior of some bioinks from the literature is predicted. By using proposed model one could choose the material based on the best predicted printability. Also one could potentially optimize the operational parameters of the 3D printers for complex and expensive materials.

Governing equations and boundary conditions

The fluid flow is assumed to be two dimensional, laminar, incompressible, isothermal and unsteady. Two phases involved in present study are immiscible. The governing equations [11, 12] in the case of two-phase flow dynamics, consists of continuity equation for material and air phases (Eqs. (1-2)) and momentum transfer equation (Eq. (3)) which is solved for the mixture of the phases. Volume fraction of each phase is tracked though volume fraction transport equation (Eq. (8)).

$$\frac{\partial(\alpha_m \rho_m)}{\partial t} + \nabla \cdot (\alpha_m \rho_m \mathbf{v}_m) = 0 \tag{1}$$

$$\frac{\partial(\alpha_a \rho_a)}{\partial t} + \nabla \cdot (\alpha_a \rho_a \mathbf{v}_a) = 0 \tag{2}$$

$$\frac{\partial(\rho \mathbf{v})}{\partial t} + \nabla \cdot (\rho \mathbf{v} \mathbf{v}) = -\nabla p + \nabla \cdot \left[\mu \left(\nabla \mathbf{v} + (\nabla \mathbf{v})^T \right) \right] + \rho \mathbf{g} + \mathbf{F}$$
(3)

$$\phi = \alpha_m \phi_m + (1 - \alpha_m) \phi_a \quad (\phi = \mu, \mathbf{v}, \text{ or } \rho)$$
(4)

$$\mathbf{F} = \frac{\gamma(\rho\kappa\nabla\alpha_m)}{0.5(\rho_m + \rho_a)} \tag{5}$$

$$\kappa = -\nabla \cdot \mathbf{n} \tag{6}$$

$$\mathbf{n} = \mathbf{n}_{\mathbf{w}} \cos \theta + \mathbf{t}_{\mathbf{w}} \sin \theta \tag{7}$$

$$\frac{\partial \alpha_m}{\partial t} + \nabla \cdot (\alpha_m \mathbf{v}) = 0 \tag{8}$$

where ρ , ρ_m , ρ_a , \mathbf{v} , \mathbf{v}_m , \mathbf{v}_a , p, \mathbf{g} , μ , α_m , α_a , and \mathbf{F} are the fluid mixture density, material density, air density, fluid mixture velocity vector, material velocity vector, air velocity vector, pressure, gravity vector, fluid mixture viscosity, material volume fraction, air volume fraction, and interfacial force vector, respectively.

For the fluid mixture properties, and interfacial force calculations, Eqs. (4) and (5) [13] were used. In Eq. (4), ϕ can be replaced by either μ , \mathbf{v} or ρ , and κ (Eq. 5) is obtained based on Eqs. (6) and (7). Here, $\mathbf{n}, \mathbf{n_w}, \mathbf{t_w}, \theta, \kappa$, and γ are the unit vector, the normal unit vector to the wall, the tangential unit vector to the wall, the fluid-wall contact angle, interface curvature and the fluid-fluid interfacial tension, respectively.

In Figure 1(a), the full physical domain has been shown (with the nozzle filled with bioink in red and the domain outside the nozzle showing air in blue as initial condition). A half domain is considered for the present analysis to make simulations computationally efficient. The results for the full physical domain are shown by mirroring the simulation output along the symmetry plane. The computational domain with dimensions used in this study is shown in Figure 1(b). The inner diameter of the nozzle at the nozzle outlet is denoted as d. Domain dimensions (30d and 60d) are selected such that flow just outside the nozzle is not affected by the boundaries.

The boundary conditions are as follows:

Inlet:
$$v_x = 0, v_y = v_\infty, \alpha_m = 1$$
 (9)

Symmetry:
$$\frac{\partial \alpha_m}{\partial x} = 0, v_x = 0, \frac{\partial v_y}{\partial x} = 0$$
 (10)

Nozzle Wall:
$$\frac{\partial \alpha_m}{\partial s} = 0, v_x = 0, v_y = 0$$
 (11)

Outlet:
$$\frac{\partial \alpha_m}{\partial y} = 0, \frac{\partial v_y}{\partial y} = 0, \frac{\partial v_x}{\partial y} = 0$$
 (12)

Side Wall:
$$\frac{\partial \alpha_m}{\partial x} = 0, v_y = 0, \frac{\partial v_x}{\partial x} = 0$$
 (13)

Upper Wall:
$$\frac{\partial \alpha_m}{\partial y} = 0, v_x = 0, \frac{\partial v_y}{\partial y} = 0$$
 (14)

The initial conditions are as follows:

Nozzle Volume:
$$\alpha_m = 1$$
 (15)

Remaining Volume:
$$\alpha_m = 0$$
 (16)

where v_x and v_y represent fluid mixture velocity in x and y directions and s represents perpendicular direction to the nozzle wall.

Geometry and mesh were created using the blockMesh utility in OpenFOAM. In the present analysis, a hexahedral block-structured grid is generated for the simulations. A grid independence test has been carried out to determine the optimum mesh resolution, providing trade-off between accuracy and computational time. Various meshes with total cell counts of 17,384, 34,512, and 69,536 were tested. Evaluated parameter was droplet break up time for water (with a nozzle inner diameter of 410 μ m). No significant effect of mesh size was observed on droplet breakup time. Therefore, the medium size mesh with total cell count 34512 cells was selected for the simulations. The mesh of the computational domain is shown in Figure 2. The mesh refinement is denser towards the nozzle wall. The smallest grid size is 0.167d. Inside the nozzle, the mesh size is uniform in the horizontal direction (0.167d), while in the vertical direction it varies from 0.167d to 0.32d. The mesh refinement is designed to ensure that the droplet is resolved with at least three cells spanning the nozzle radius at the exit, where droplet formation occurs.

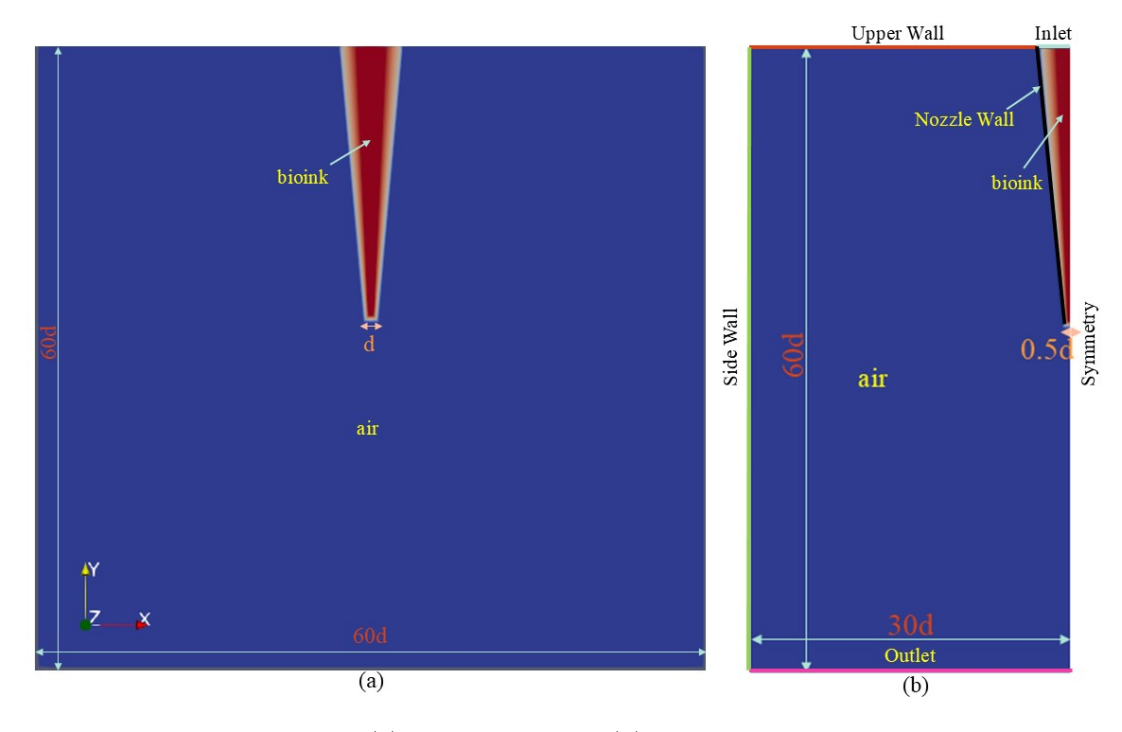


Figure 1. (a) Full domain and (b) Computational domain

Solution methodology

In present study, VOF method is used within FVM framework [14], where FVM solves the governing equations, and VOF tracks the fluid interfaces [7]. For each cell in the computational domain, VOF tracks the volume fraction of each fluid. A volume fraction value of 0 indicates that the cell contains no biomaterial, while a value of 1 indicates that the cell is completely filled with biomaterial. For cells at the interface where the two fluids meet, the volume fraction lies between 0 and 1. Free surface is defined by volume fraction 0.5. The interFoam solver in OpenFOAM is used for the simulations. Pressure-velocity decoupling is avoided by employing the PIMPLE algorithm, which is a combination of PISO (Pressure Implicit with Splitting of Operator) and SIMPLE (Semi-Implicit Method

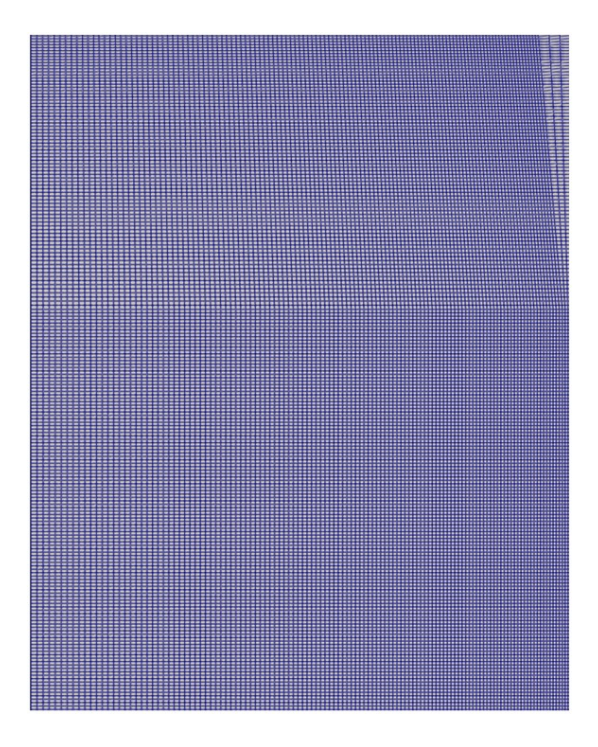


Figure 2. Mesh of the computational domain

for Pressure-Linked Equations). To discretize the gradient, divergence and Laplacian terms in the governing equations, the central differencing scheme, second order upwind scheme and central differencing scheme are used. The Courant number was taken as 1. For time discretization, the Euler scheme was employed. The convergence criterion of continuity, and momentum equations was set to 10^{-6} .

Simulation setup for materials

Materials and parameters

Biomaterial properties are taken from [4] and [8]. Since surface tension(σ) data has not mentioned in aforementioned papers, surface tension data are taken as 58 mN/m [9] and 45 mN/m [10]. The materials, their properties (ρ_m , viscosity model, K, n, τ_0 , σ) and other parameters (d) used in the present analysis are listed in Table 1. The printing speed for biomaterials used in the present analysis is 8 mm/s [4]. Printing speed used for water is specified in a subsequent section.

Viscosity models

The viscosity models used in this study to predict the viscosity behavior of biomaterials are Power law model Eq. (17) and Herschel–Bulkley model Eq. (18), with expressions as follows:

$$\mu_m = K\dot{\gamma}^{n-1} \tag{17}$$

$$\tau = \tau_0 + K\dot{\gamma}^n \tag{18}$$

where $\mu_m, K, \dot{\gamma}, n, \tau$, and τ_0 represent dynamic viscosity of material, flow consistency index, shear rate, flow behavior index, shear stress and yield stress respectively.

Table 1. Simulation parameters.

Biomaterial	$\rho_m(\mathrm{g/mL})$	viscosity model	K	n	$\tau_0(\mathrm{Pa})$	$\sigma({ m N/m})$	d(mm)
GelMA30 at RT	1.30	Herschel-Bulkley	0.01	0.82	0.04	0.045	200[4]
GelMA60 at $16^{\circ}\mathrm{C}$	1.05	Power law	14.3	0.119	-	0.045	250[8]
GelMA60 at RT	1.05	Power law	0.0164	0.141	-	0.058	200
GelMA 5% w/v	1.05	Herschel-Bulkley	0.73	0.41	0.07	0.045	200
Water	1	Newtonian	-	-	-	0.072	410

Non-dimensional numbers

To study the effects of different parameters on the flow behavior of Newtonian materials outside the nozzle using the present model, non-dimensional numbers, Reynolds number (Re) and Weber number (We) (Eqs. (19) and (20)) are used in the analysis. These non-dimensional numbers help to demarcate flow regimes based on the material flow behavior outside the nozzle.

$$Re = \frac{\rho_m V l}{\mu_m} \tag{19}$$

$$We = \frac{\rho_m V^2 l}{\sigma} \tag{20}$$

Here ρ_m , V and l are material density, printing speed and characteristic length (0.5d), respectively.

Results and discussion

Comparison of model with literature

The comparison between the model results and experimental data from the literature for GelMA60 at 16°C and GelMA30 is shown in Figure 3a and Figure 3b, respectively. The model's prediction for the coherent nature of GelMA60 fiber at 16°C and the droplet fiber for GelMA30 at room temperature (RT) aligns well with literature data. Hence, the proposed VOF model is employed to predict the flow behavior of both Newtonian and non-Newtonian materials outside the nozzle in the following sections.

Results with Newtonian material

Simulations are carried out for water with a nozzle inner diameter of 410 mm with different Re and We. Simulation parameters and flow regimes based on flow outside the nozzle are shown in Table 2. Contour plots for a representative case (Re = 9.39, We = 0.0059) of bubble formation, growth, breakup, propagation and formation of new bubble in the dripping regime are shown in Figure 4. The legend alpha.water represents the volume fraction of water in the domain. The dripping regime has been observed until Re = 80, We = 0.4, beyond which flow instability is detected (Figure 5a-5c). Initially, the flow gets elongated up to Re = 117.42, We = 0.93 (Figure 5a). After that continuous bubble near the outlet are observed until Re = 234.85, We = 3.73 (Figure 5b). This regime is termed as transitional regime. Critical Reynolds and Weber numbers are reached at Re = 317.04, We = 6.81, respectively (Figure 5b). Eventually, the flow enters in jetting regime (Figure 5d) at Re = 352.27, We = 8.41 where uninterrupted flow can be seen.

Table 2. Flow regime data for water.

Printing Speed (m/s)	Re	We	Regime
0.046	9.39	0.0059	Dripping
0.20	41.09	0.11	Dripping
0.37	76.33	0.39	Dripping
0.50	103.33	0.72	transitional
0.57	117.42	0.93	transitional
1.15	234.85	3.73	transitional
1.55	317.04	6.81	Jetting starts
1.72	352.27	8.41	Jetting

Table 3. Printability prediction of biomaterials.

Biomaterial	Nature of fiber	Printability Prediction
GelMA60 at RT GelMA60 at 16°C GelMA 5% w/v GelMA30 at RT	droplet fiber Continuous fiber Continuous fiber droplet fiber	not printable(NP) printable(P) P NP

Results with non-Newtonian material

Simulations are performed for biomaterials listed in Table 1. The predicted nature of the fiber and the printability of these biomaterials are reported in Table 3. The predicted filament shapes for GelMA60 at RT and GelMA 5% w/v are shown in Figure 6a and Figure 6b, respectively. Biomaterials that form droplet-shaped filaments are deemed unprintable, whereas those that form continuous fibers are printable [8]. These criteria are used to determine the printability based on the filament shape. The same biomaterial may become printable with a change in temperature (Table 3) due to the dependence of its rheological properties on temperature. The flow behavior for GelMA60 at different temperatures are shown in Figure 3a at 16°C and Figure 6a at RT respectively. In the case of GelMA60, it became printable at lower temperature [8]. The current computational model could be further improved by incorporating the temperature variation of the biomaterial's rheological properties. Additionally, the model currently uses time-averaged viscosity models (Power Law and Herschel-Bulkley), and its accuracy could be enhanced by adopting time-dependent viscosity models.

Conclusions

The present study has utilized a multiphase numerical model solved by VOF method under FVM framework which aims to analyze the flow behavior of bioinks outside the 3D printing nozzle. The model predictions for the flow behavior of GelMA materials at different temperatures matches well with experimental data from the literature. Hence model can capture the flow dynamics of bioinks. Proposed model can be used for further applications in 3D printing.

The simulations identified distinct flow regimes for water, with critical Reynolds and Weber numbers identified. This study for water can serve as base study for bioinks (non-Newtonian). Understanding of these regimes is important for designing the print-

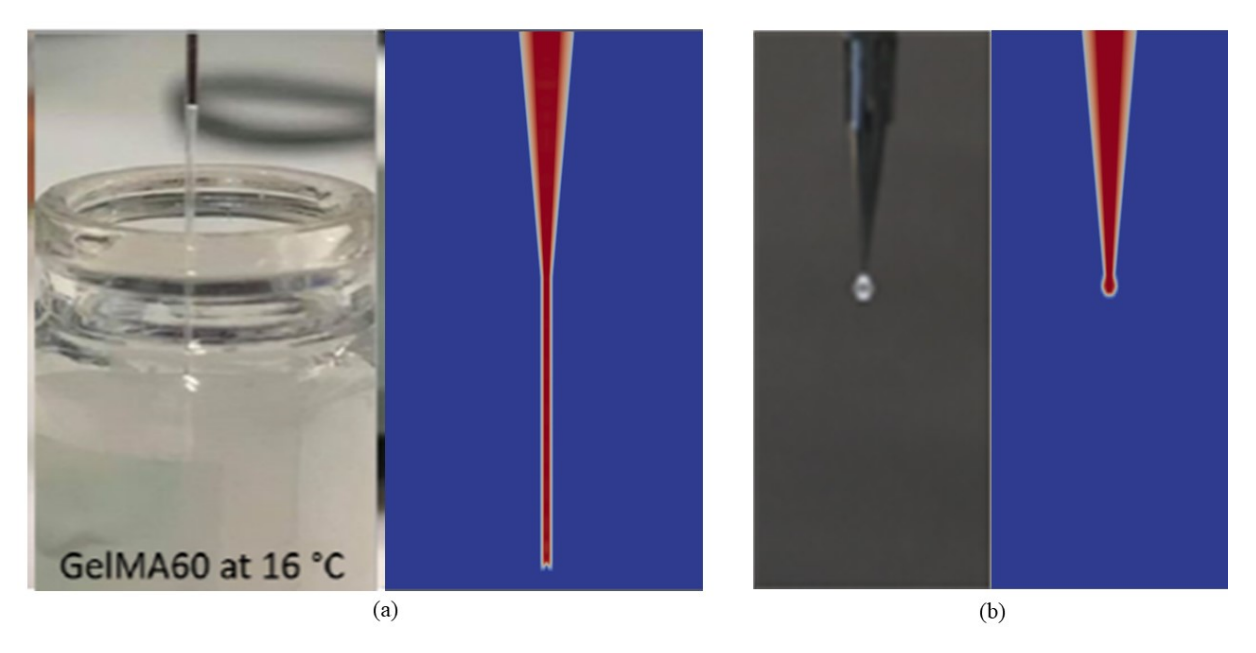


Figure 3. Comparison of model and experiment data from literature for (a) GelMA60 at 16° C [8] and (b) GelMA30 [4]

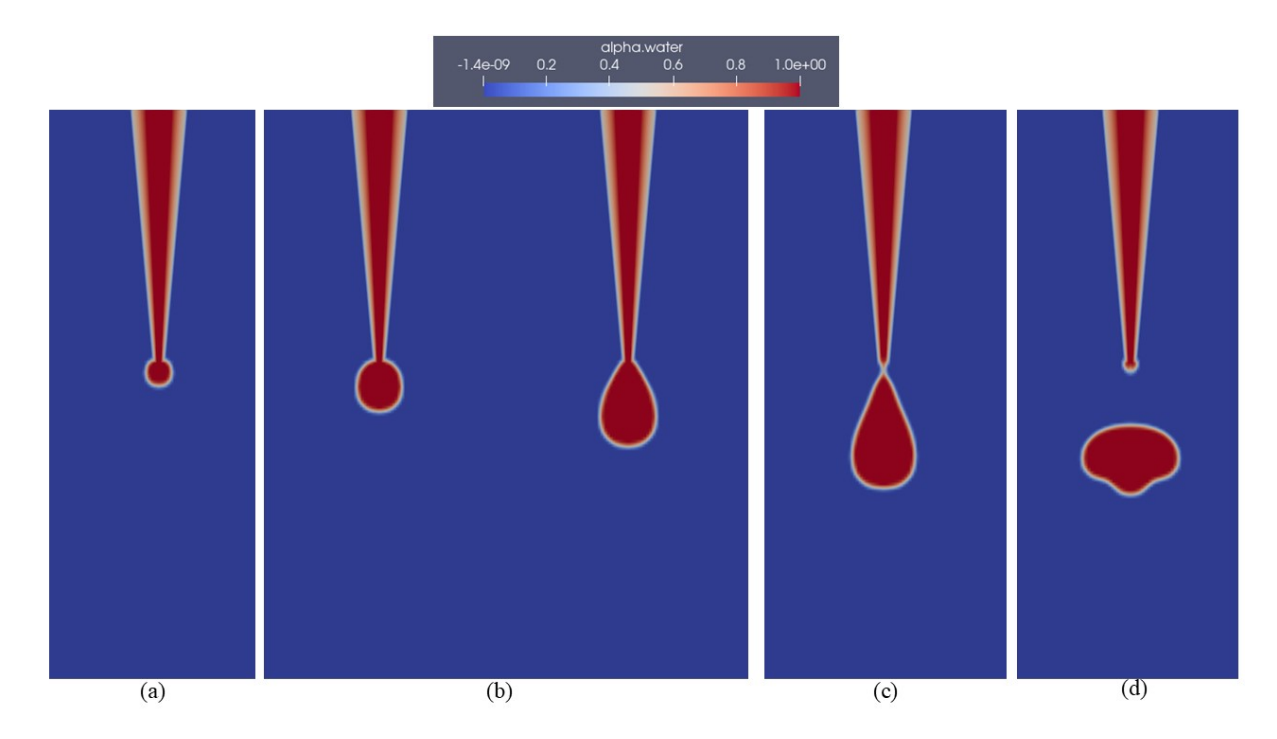


Figure 4. Contour plots of bubble (a) formation (b) growth (c) breakup (d) propagation and new bubble formation in dripping regime for water

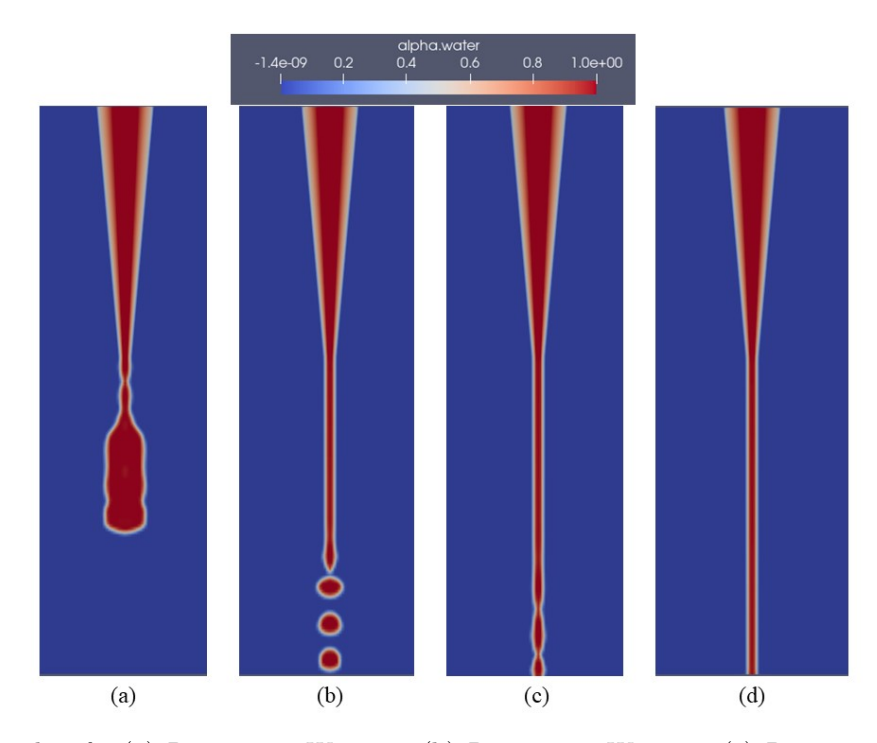


Figure 5. Contour plots for (a) Re=117.42, We=0.93 (b) Re=234.85, We=3.73 (c) Re=317.04, We=6.81 and (d) Re=352.27, We=8.41 for water

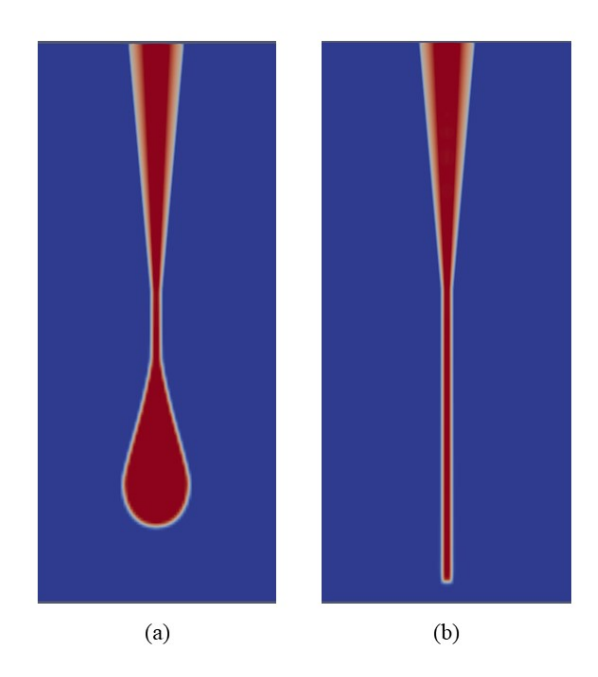


Figure 6. Predicted filament shape for (a) GelMA60 at RT and (b) GelMA $5\%\,$ w/v

ing process for non-Newtonian materials. This can help in more precise and controlled drug formulations. The present study indicates that rheological properties affects bioinks significantly. The predictive capability of the proposed model can facilitate the design of bioinks with tailored characteristics without going for actual experimentation. This can save time and cost of the actual physical experimentation.

Temperature significantly affects printability, as seen with GelMA60. While the current model is effective, it can be improved by incorporating temperature-dependent rheological properties for enhanced accuracy. The computational framework of model given in this study will be useful for future research in prediction of flow behavior of complex materials. Instead of time averaged viscosity models, time dependent viscosity model can be used in the present model to predict recovery behavior of bioinks. Present model can be extended in three dimension to study stackability of bioink on the flat plate. 3D printing path planning can be done by such model. 3D printing of various shapes can be assessed well in advance by such three dimensional model. Stackability of drug shapes having multilayer non-Newtonian materials can be checked with three dimensional model.

Acknowledgments

This research was carried out using financial support from 3D-CURE project at TUAS. The 3D-CURE project was funded by Business Finland. The authors are thankful to Dr. Sanna Turunen (TUAS NMP) for her insightful discussions. During this work, the high-performance computing resources were provided by CSC-IT Center for Science Ltd, in Espoo, Finland.

References

- [1] Bodnar, T., Sequeira, A., Analysis of the shearthinning viscosity behavior of the johnson segalman viscoelastic fluids. Fluids, 7(1), 36, 2022. https://doi.org/10.3390/fluids7010036
- [2] Fatemeh Ardaneh, Eero Immonen, Jani Pelkonen, Santeri Knuutinen, Ashvinkumar Chaudhari, Analysis of Viscosity Behaviour of Shear-Thining Hydrogels in 3D-Printing Nozzles. *Communications of the ECMS*, 38(1), 2522–2414, 2024. https://doi.org/10.7148/2024-0359
- [3] Ratnesh Raj, Siriki Vamsi Venkata Krishna, Akshat Desai, Chintapalli Sachin, and Amit Rai Dixit, Print fidelity evaluation of PVA hydrogel using computational fluid dynamics for extrusion dependent 3D printing. *IOP Conf. Ser.: Mater. Sci. Eng.*, 1225, 012009, 2022. https://doi:10.1088/1757-899X/1225/1/012009
- [4] H. Jongprasitkul, S. Turunen, V. S. Parihar, M. Kellomaki, Sequential Cross-linking of Gallic Acid-Functionalized GelMA-Based Bioinks with Enhanced Printability for Extrusion-Based 3D Bioprinting. *Biomacromolecules*, 24 (1), 502–514, 2023. https://doi.org/10.1021/acs.biomac.2c01418
- [5] Piotr Cendrowski, Katarzyna Kramek-Romanowska, Dorota Lewinska, Marcin Grzeczkowicz, Paulina Korycka, Jan Krzysztoforski, CFD modeling of droplet generation process for medical applications using the electrostatic impulse method. *Chemical and Process Engineering*, 43(3), 335–355, 2022. http://dx.doi.org/10.24425/cpe. 2022.142278

- [6] Farzad Liravi, Robin Darleux, Ehsan Toyserkania, Additive manufacturing of 3D structures with non-Newtonian highly viscous fluids: Finite element modeling and experimental validation. *Additive Manufacturing*, 13, 113–123, 2017. https://doi.org/10.1016/j.addma.2016.10.008
- [7] C.W. Hirt and B.D. Nichols, Volume of fluid (VOF) method for the dynamics of free boundaries. *Journal of Computational Physics*, 39(1), 201–225, 1981. https://doi.org/10.1016/0021-9991(81)90145-5
- [8] Hatai Jongprasitkul, Sanna Turunen, Vijay Singh Parihar, Shambhavee Annurakshita, and Minna Kellomaki, Photocross-linkable Methacrylated Polypeptides and Polysaccharides for Casting, Injecting, and 3D Fabrication. *Biomacromolecules*, 22 (2), 481–493, 2020. https://doi.org/10.1021/acs.biomac.0c01322
- [9] Elkhoury K, Sanchez-Gonzalez L, Lavrador P, Almeida R, Gaspar V, Kahn C, Cleymand F, Arab-Tehrany E, Mano JF, Gelatin Methacryloyl (GelMA) Nanocomposite Hydrogels Embedding Bioactive Naringin Liposomes. *Polymers*, 12(12), 2944, 2020. https://doi.org/10.3390/polym12122944
- [10] R. Kadri, G. Ben Messaoud, A. Tamayol, B. Aliakbarian, H. Y. Zhang, M. Hasan, L. Sanchez-Gonzalez, and E. Arab-Tehrany, Preparation and characterization of nanofunctionalized alginate/methacrylated gelatin hybrid hydrogels. *RSC Advances*, 6, 27879–27884, 2016.
- [11] I.L. Chaves, L. Duarte, W.K.T. Coltro, and D.A. dos Santos, Droplet length and generation rate investigation inside microfluidic devices by means of CFD simulations and experiments. *Chemical Engineering Research and Design*, 161, 260–270, 2020. https://doi.org/10.1016/j.cherd.2020.07.015
- [12] Christian Mulbah, Can Kang, Ning Mao, Wei Zhang, Ali Raza Shaikh, and Shuang Teng, A review of VOF methods for simulating bubble dynamics. *Progress in Nuclear Energy*, 154, 104478, 2022. https://doi.org/10.1016/j.pnucene.2022.104478
- [13] Brackbill, J.U., Kothe, D.B., Zemach, C., A continuum method for modeling surface tension. *J. Comput. Phys.*, 100, 335–354, 1992. https://doi.org/10.1016/0021-9991(92)90240-Y
- [14] S. Patankar, Numerical Heat Transfer and Fluid Flow. CRC Press, 2018.

Ashish Pawar, Ashvinkumar Chaudhari and Eero Immonen Computational Engineering and Analysis Turku University of Applied Sciences 20520 Turku, Finland